Original Article

Journal of Drought and Climate change Research (JDCR)

Summer 2025, Vol. 3, No. 10, pp 19-36

10.22077/jdcr.2025.8877.1113

Eco-Friendly Synthesis of Magnetic NiFe2O4-Chitosan Nanocomposite for Cyanide Removal: A Sustainable Strategy for Water Resource Management

Fatemeh Deymeh[1], Ahmad Hajizadeh[1], Ali Zeraatkar Moghaddam [*,1]

1-Department of Chemistry, Faculty of Science, University of Birjand, Birjand, Iran.

***Corresponding Author: a_zeraatkar_m@birjand.ac.ir**

Keywords:
Climate change, Water resource management, Green Magnetic NiFe2O4, Chitosan, Cyanide removal

Abstract

The growing issue of water scarcity, exacerbated by climate change and extended droughts, underscores the critical need for effective water and wastewater treatment strategies. In this study, NiFe2O4 magnetic nanoparticles were synthesized using a green synthesis approach in peppermint (Mentha) extract medium, ensuring an eco-friendly fabrication process. The magnetic nanoparticles were coated and modified with chitosan, resulting in a new nanocomposite with improved adsorption properties. This green-synthesized magnetic chitosan nanocomposite was characterized using FTIR, XRD, VSM, SEM, and TEM, and subsequently applied to remove cyanide from contaminated groundwater and industrial wastewater. The adsorption process was optimized through an experimental design procedure, achieving a maximum removal efficiency of 97.1 ± 3.8% at a 95% confidence level, closely matching the experimental results of 95.8 ± 7.7%. The results highlight the potential of this sustainable nanocomposite for water and wastewater treatment, aiding effective water resource management in the face of climate change and growing water scarcity.

Received:
02 February 2025

Revised:
27 March 2025

Accepted:
11 April 2025

How to cite this article:
Deymeh, F., Hajizadeh, A., & Zeraatkar Moghaddam, A. (2025). Eco-Friendly Synthesis of Magnetic NiFe2O4-Chitosan Nanocomposite for Cyanide Removal: A Sustainable Strategy for Water Resource Management. *Journal of Drought and Climate change Research* (JDCR), 3(10), 19-36. 10.22077/jdcr.2025.8877.1113

Introduction

Various industries, especially mining, pharmaceuticals, and agriculture, use cyanide (CN-) compounds (Kuyucak & Akcil, 2013). As an essential ingredient in mining, cyanide facilitates the dissolution of Au and Ag silver through complexation reactions (reactions 1 and 2).

$$2Ag + 4CN^- + 1/2\ O_2 + H_2O \rightleftharpoons 2[Ag(CN)_2]^{-1} + 2OH^- \quad (1)$$

$$2Au + 4CN^- + 1/2\ O_2 + H_2O \rightleftharpoons 2[Au(CN)_2]^{-1} + 2OH^- \quad (2)$$

However, despite its industrial significance, cyanide is highly toxic, posing serious environmental and health hazards which can cause severe health complications even at concentrations as low as 0.2 $mg.L^{-1}$ (Dash et al., 2009a). Small amounts of cyanide can deactivate cytochrome oxidase, which ultimately prevents the so-called cellular respiration, which ultimately causes tremors, nerve damage, and eventually death (Beasley & Glass, 1998; Gracia & Shepherd, 2004; Hendry-Hofer et al., 2019). Due to this, they are commonly found in wastewater generated by these industries, posing significant environmental risks (Moussavi & Khosravi, 2010; Singh & Balomajumder, 2016). Given these risks and the extensive industrial use of cyanide, large quantities of cyanide-laden wastewater are continuously released into the environment, necessitating efficient and sustainable treatment methods.

Usually, cyanide-containing wastewater is treated by alkaline chlorination, which uses chlorine to convert cyanide into cyanogen chloride and sodium cyanate as intermediates, eventually converting them into non-toxic end products, i.e. CO2 and N2 (Dash et al., 2009a). This method effectively lowers cyanide levels; however, it creates toxic sludge and incurs high operational costs. Furthermore, chlorinated by-products may form when this sludge reacts with organic compounds in wastewater. Due to these limitations, there is a crucial need for alternative cyanide remediation strategies that are both cost-effective and environmentally sustainable.

Electrochemical techniques (Hassani et al., 2011; Scarazzato et al., 2015), ozone treatment (Chang et al., 2008), wet-air oxidation (WAO), and "acidification/ volatilization/re-neutralization" (AVR) have also been utilized as CN- remediation alternatives. Electrochemical and WAO techniques are limited to small-scale operations (Pulkka et al., 2014), while ozonation equipment is prohibitively expensive. The use of biological methods is severely limited by the microbial and cytotoxicity of cyanide, owing to the strong complexation tendency of metals and cyanide, inactivating live-essential metalloenzymes (Luque-Almagro et al., 2016). The removal of cyanide with adsorbents has been proven to be rather effective. Adsorbents are advantageous due to their low cost, insensitivity to cyanide's toxicity, inherent simplicity, and reusability. Removal of cyanide has been reported using sorbents from agricultural wastes, including nutshells, coconut husks, calcinated eggshells (Eletta et al., 2016), rice husks (Yazici et al., 2009), pistachios' green hulls (Moussavi & Khosravi, 2010), guar gum (Sharma, Kumar, Devi, et al., 2018), and by activated carbon (Singh & Balomajumder, 2016; Zhang et al., 2010) and activated carbon modified by TiO2 (Ramírez-Muñiz et al., 2010).

As a result of their many advantageous properties, biopolymers like chitosan and gums have been intensively investigated (Bhatnagar & Sillanpää, 2009; Kumar et al., 2017; Sharma et al., 2018a; Sharma et al., 2018b). Compared to activated carbon, chitosan has a much greater concentration of hydroxyl groups on its surface, making it an excellent candidate for pollutant removal (Bhatnagar & Sillanpää, 2009). However, like all polysaccharides, it is not easy to remove it from the purified effluents (Reddy & Lee, 2013). Linking chitosan and other compounds to magnetic particles is a solution for environmental remediation, which allows for a simple, cheap, energy-efficient, and rapid water treatment (Donia et al., 2008; Hritcu et al., 2012; Moghaddam et al., 2020; Shadman et al., 2021; Tanhaei et al., 2015). Such magnetic sorbents can be removed from the solution using magnets. Iron oxide is most commonly used as the magnetic core for the preparation of such chitosan-based adsorbents (Pisanic et al., 2007), but other magnetic particle polymer combinations have been studied (Reddy & Lee, 2013). Iron oxides are unstable at low pH, which impairs their capability to be magnetically separated. Protecting the cores with an inert layer remedies this drawback whilst potentially providing another layer for improved sorption (Wang et al., 2010).

This study addresses the need for cost-effective and eco-friendly remediation techniques using a green-synthesized NiFe2O4-chitosan nanocomposite for cyanide removal. The study highlights the nanocomposite's potential as an effective and environmentally responsible adsorbent, offering an alternative to conventional treatments that frequently generate hazardous byproducts. The results contribute to more sustainable environmental protection strategies by providing insightful information on new cutting-edge materials for wastewater treatment.

Materials and Methods

Chemicals

Sodium cyanide (NaCN) and chitosan were acquired from Sigma–Aldrich Co (St. Louis, United States). All solvents were analytical grade and purchased from Merck Co. (Darmstadt, Germany). Hydrochloric acid (HCl, 37%), sodium hydroxide (NaOH, 99%), nickel chloride hexahydrate ($NiCl_2 \cdot 6H_2O$, 98%), ferric chloride hexahydrate ($FeCl_3 \cdot 6H_2O$, 98%), and glutaraldehyde (25% aqueous solution) were provided by Merck Co. (Darmstadt, Germany). Double-distilled deionized water (DDW) was used in all experiments and cleaning procedures unless mentioned otherwise. The concentrations of chemical solutions and their preparation methods are detailed in the respective synthesis sections.

Instruments

A JASCO 4600 series FT-IR spectrometer (Tokyo, Japan) was used for Fourier-transform infrared spectroscopy (FT-IR), conducted at room temperature with a scanning range of 400–4000 cm^{-1}, utilizing KBr pellets. X-ray diffraction (XRD) patterns were obtained using a Bruker AXS-D8 diffractometer (Billerica, Massachusetts, United States) with Cu-$K\alpha_1$ radiation (λ = 1.5406 Å) at a step size of 0.02° and a scanning rate of 1°/min. The microstructure of the synthesized composites was analyzed via scanning electron microscopy (SEM) and transmission electron microscopy (TEM) using a Philips CM-30 TEM (Eindhoven, Netherlands). The magnetic properties were assessed with a Lake Shore VSM model 7400 (Westerville, USA) under an applied field of ±10 kOe.

Synthesis of proposed green nanocomposite

Using mint extract as a natural reducing agent, a green synthesis method for NiFe2O4 nanoparticles is performed according to the literature with some modifications (Kalita et al., 2022). Fresh mint leaves (10 mg) were thoroughly washed with DDW and boiled in 100 mL of DDW at 80°C for 30 minutes, and the resulting extract was filtered using a Whatman No.1 filter paper and stored at 4°C for further use.

For green synthesis of NiFe2O4 nanoparticle, the solutions containing NiCl2.6H2O (0.1 M) and FeCl3.6H2O (0.2 M) were separately prepared in DDW (Kalita et al., 2022; Zeraatkar Moghaddam et al., 2018). Then, 50 mL of the mint extract was slowly added dropwise to the prepared solutions while stirring continuously. The mixture was subjected to 90°C for 2 hours to facilitate the reduction of metal ions and nanoparticle formation. Afterward, the precipitate was separated via centrifugation (6000 rpm, 10 min), washed with DDW to remove any remaining impurities, and dried at 100°C overnight. Ultimately, the obtained powder was calcined at 450°C for 2 hours to enhance crystallinity and structure integrity. This method offers an eco-friendly technique for producing NiFe2O4 nanoparticles, which may be utilized in water treatment and environmental remediation (Kalita et al., 2022; Zeraatkar Moghaddam et al., 2018).

After the NiFe2O4 was prepared and collected, 1.0 g of chitosan was dissolved in an 2% (v/v) aqueous acetic acid solution (Zeraatkar Moghaddam et al., 2018). Next, 0.5 g of the green synthesized NiFe2O4 nanoparticles were added and sonicated for 30 min to ensure uniform dispersion. Then, 5 mL of an aqueous 25% (w/v) glutaraldehyde solution was blended with the mixture to initiate gelation, followed by drying in a forced convection oven at 60°C overnight. Before grinding, the composite particle gels were washed several times with an aqueous acetic acid (2% (v/v)) solution and double distilled water, then dried at 50°C for another 12 hours (Tanhaei et al., 2015; Zeraatkar Moghaddam et al., 2018). They were kept under low humidity conditions in a desiccator to preserve the particles for further use.

Adsorption and desorption experiments

Adsorption experiments were conducted in batch mode, i.e., a defined amount of adsorbent (15-75 mg) and cyanide pollutant (100 to 200 $mg.L^{-1}$) was mixed in 10 mL water (temperature 25°C), whose pH-value was set to predefined values between 7 and 11 by 0.01 M HCl or NaOH aqueous solutions, depending on the experiment. The contact time was between 10 and 30 min under stirring at 800 rpm. After that, the adsorbents were separated from the remainder of the suspension, followed by quantification of the remaining cyanide in the solution. In all cases, titration was used to obtain cyanide concentrations (C), utilizing AgNO3 (0.001M) and aqueous potassium iodide (10 g/L) solutions as indicators.

A similar approach was used in isothermal studies with cyanide concentrations between 10 and 500 $mg.L^{-1}$ and 60 minutes of contact time. In kinetic studies, 50 $mg.L^{-1}$ cyanide was used with contact times between 1 and 35 min with the other parameters at optimized values. After reaching equilibrium, removal efficiency and adsorption capacity values (qe and qt (mg. g-1), respectively) were determined using Eqs. 3 and 4 (Sadeghi et al., 2015; Shadman et al., 2021; Tanhaei et al., 2015).

$$Cyanide\ removal\ (\%) = \frac{(C_0 - C_e)}{C_e} \times 100 \qquad (3)$$

$$q_e = \frac{(C_0 - C_e)V}{m} \; and \; q_t = \frac{(C_0 - C_t)V}{m} \quad (4)$$

where Co (mg L-1), Ce (mg L-1), and Ct (mg L-1) stand, respectively, for the initial (o), equilibrium (e), and time-dependent (t) cyanide ion concentrations. m (g) stands for the mass of the proposed nanocomposite, and V (L) is the solution volume used.

Optimization of the treatment process

The adsorbent works reasonably well under most not-too-acidic conditions. However, major process factors were optimized, namely contact time, adsorbent dosage, initial pollutant concentration, and solution pH. Temperature (298 K) and stirring rate (800 rpm) were kept constant to ensure comparability. For efficient testing, we used CCD (Design Expert 10.0.0 (Stat-Ease Inc., Minneapolis, MN, USA)) to determine a minimum of experimental conditions to optimize the experimental design.

Results and Discussion

Characterization

FTIR results of the proposed green NiFe2O4-chitosan nanocomposite (Figure 1) show typical patterns for chitosan, namely the coinciding stretching vibrations of N–H and O–H (broad absorption peak at ~3400 cm-1), indicating the presence of hydroxyl (–OH) and amine (–NH_2) groups from chitosan. The broadness of the peak suggests hydrogen bonding interactions within the composite. The stretching vibrations band at ~2924 cm-1 is associated with the C–H stretching vibrations of aliphatic groups in chitosan, confirming the organic nature of the polymeric backbone. The peak at ~1640 represents the C=O stretching vibration from amide groups (amide I band) in chitosan. This peak suggests that the chitosan structure remains intact after the synthesis process. The C–N stretching vibrations, at ~1380 cm-1, further support the presence of chitosan within the nanocomposite. Moreover, a strong peak at ~1100 cm-1 shows the characteristic of the C–O–C stretching vibrations, confirming the glycosidic bond structure in chitosan. Finally, A prominent peak around 580 cm-1 is attributed to the Fe–O and Ni–O stretching vibrations, confirming the successful formation of NiFe2O4 nanoparticles. Thus, FTIR suggests the successful formation of nanocomposite consisting of nickel ferrite, chitosan, and glutaraldehyde.

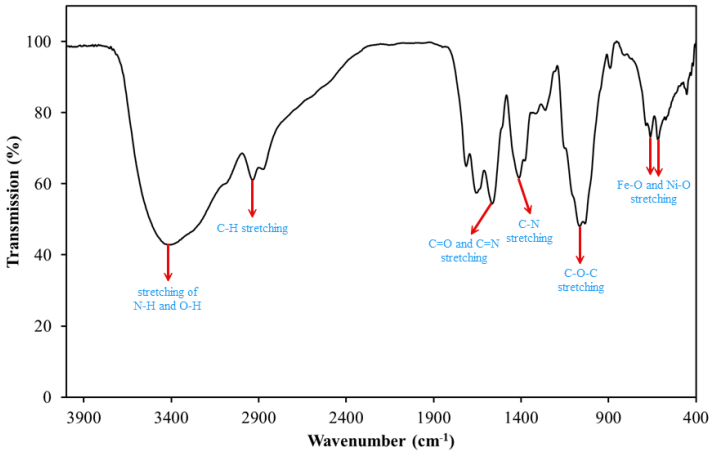

Fig 1. FTIR spectrum of proposed green $NiFe_2O_4$-chitosan nanocomposite.

A vibration sampling magnetometry (VSM) analysis of the green prepared NiFe2O4-chitosan nanocomposite shows a significant reduction in magnetization compared to pure green synthesized NiFe2O4 (see Fig. 2). Because glutaraldehyde cross-linked chitosan is non-magnetic, it forms an insulating layer around the magnetic core, limiting direct magnetic interactions. Despite this reduction in magnetization, the residual magnetic field remains sufficient to allow effective magnetic separation (see Fig. 2) (Jacob et al., 2011).

X-ray diffraction shows a rather complex pattern consisting of sharp peaks stemming from green NiFe2O4 (Kalita et al., 2022) (Figure. 3). The peaks at 2θ=18.5°(111), 30.3°(220), 35.9°(311), 37.3°(222), 43.5°(400), 53.9°(422), 57.7°(511), and 63.1°(440) can be indexed to the Miller indices in the brackets behind the respective reflections according to JCPDS-card no. 10-0325 of cubic nickel ferrite. The observed peaks are at slightly higher 2θ than the JCPDS-reference (ca. 0.1°), which could be the consequence of the small size of the particles. In addition, a strong amorphous halo with two broad modes around 40° is prominent, which is typical for complex amorphous polymers and, thus, can be seen as the proof for the immobilization of chitosan and crosslinked glutaraldehyde on green NiFe2O4 (Kalita et al., 2022; Munir et al., 2021).

SEM image of green NiFe2O4-chitosan nanocomposite shown in Figure 4a shows porosity and agglomeration. A high-magnification image reveals interconnected nanoparticles, which increase surface area and provide more active sites for adsorption. As a result of the porous morphology observed, cyanide ions can be absorbed more effectively.

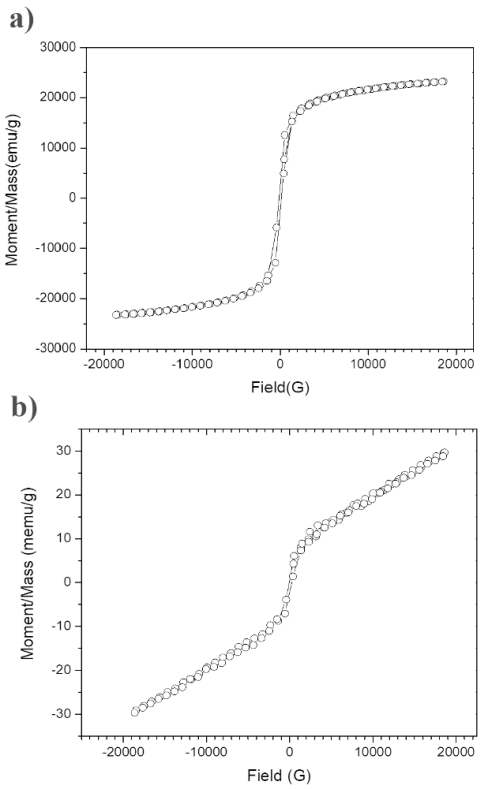

Fig 2. VSM data of the synthesized a) green NiFe2O4, and b) NiFe2O4-chitosan nanocomposite.

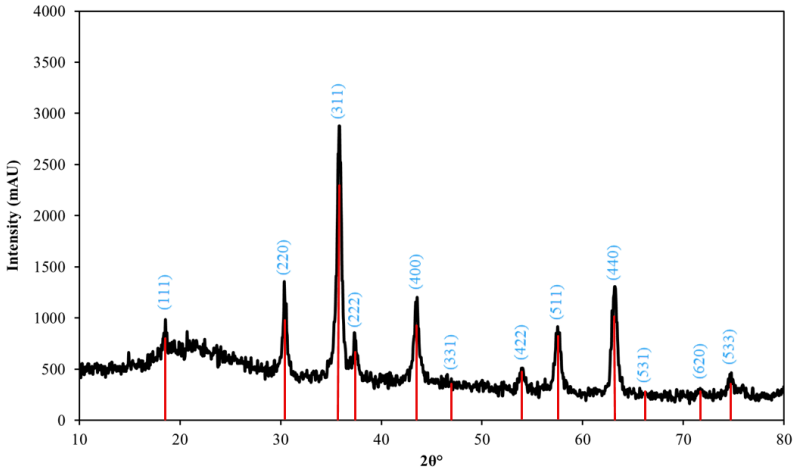

Fig 3. XRD pattern of the synthesized NiFe2O4-chitosan nanocomposite.

Figure 4b shows the TEM image of a nanocomposite particle with a well-defined dark core (green NiFe2O4) and lighter outer layer (chitosan). An approximate 100 nm particle size confirms nanoscale dimensions. In this nanocomposite, the NiFe2O4 core is encapsulated by a polymeric layer, which stabilizes the nanocomposite while maintaining sufficient magnetization for easy separation.

Experimental Design

In most experimental studies, univariate methods are used, i.e., an entire matrix of experiments is conducted, which means that many time-intensive and costly experiments are required. Furthermore, such a matrix approach does not assess variable interactions unless special advanced analysis techniques are used. A remedy to this predicament is multivariate techniques, which offer fast and efficient tools for optimizing several variables simultaneously. In this work, we use CCD, an independent quadratic design tool (Montgomery, 2019; Reece et al., 1993). The major influential parameters on cyanide adsorption are the amount of NiFe2O4-chitosan nanocomposite, contact time, pH, and initial cyanide concentration while keeping minor parameters (stirring rate, temperature) constant. These major parameters were systematically varied using a central composite design-based model to establish the parameter-performance surface, followed by variance

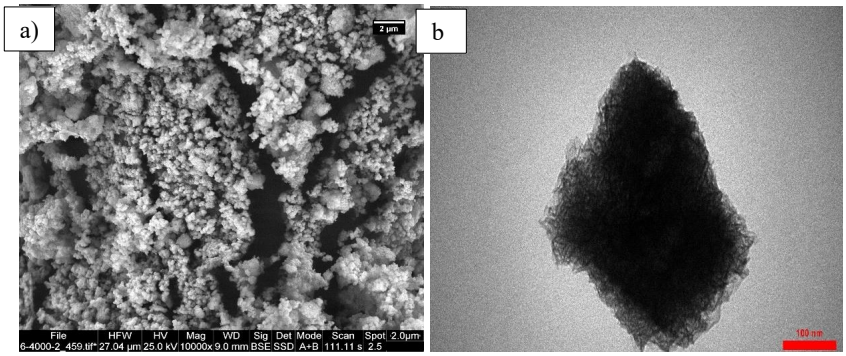

Fig 4. SEM and TEM images for the synthesized NiFe2O4-chitosan nanocomposite.

analysis (ANOVA) to find the most relevant parameters and their predictions for the optimal parameter combination (Montgomery, 2019).

As the number of optimization parameters is small enough, a simple factorial design is sufficient, allowing for the application of CCD directly (Reece et al., 1993). To assess the number of required design points N, equation 5 is used.

$$N = 2^k + 2k + N_0 \quad (5)$$

In this equation (Eq. 5), k stands for the number of input parameters, and N0 corresponds to the replicate number in the central design. Based on this equation, 36 experiments are required by the CCD, which were randomized in three blocks with four replicates per block. The values used for each of the four parameters are given in Table 1. The results of ANOVA and CCD analyses were found to be described by the quadratic polynomial, which reads as:

$$\mathrm{R}\,(\%) = +68.5 - 10.6\mathrm{A} + 13.4\mathrm{B} - 10.1\mathrm{C} + 3.5\mathrm{D} + 6.5\mathrm{AB} + 3.0\mathrm{BC} + 5.9\mathrm{A}^2 + 3.4\mathrm{C}^2 \quad (6)$$

Table 1. levels and experimental variables of the CCD.

Parameters	Levels				
	-α	-1	0	+1	+α
Initial pH (A)	7	8	9	10	11
Nanocomposite amount (mg) (B)	15	30	45	60	75
Initial concentration ($mg.L^{-1}$) (C)	12.5	25	37.5	50	62.5
Contact time (min) (D)	15	30	45	60	75

ANOVA analysis shows individual contributions from different sources to the overall experimental result variations. ANOVA results for cyanide removal in terms of their statistical significance parameters (P-values, the sum of the squares, and Fisher's F-ratios) can be found in Table 2. An F-value of 40.2 indicates a 0.01% chance of the observed result being due to statistical noise and signifies the high importance of the results (A. Asfaram et al., 2016). A p-value above 0.05 for the lack of fit suggests an excellent ability of Eq. 6 to fit the experimental data. Consequently, the quadratic A2 and C2 and the linear and interaction terms A, AB, B, BC, C, and D are statistically significant. The cyanide removal performance could be modeled with a high $R^2 = 0.9462$, showing an excellent agreement between modeled and experimental results. Moreover, the predicted $R^2 = 0.9260$ and the adjusted $R^2 = 0.8491$ conform well. Figure 5 shows the residual plot, indicating only a few percent deviations between modeled and experimental results. This shows the absence of considerable contradictions in the model, good experimental quality (low statistical scatter), and no violation of the initial assumptions. There is low statistical scatter in the residual plot (Figure 5), showing the model's high accuracy, denoted by an excellent signal-to-noise ratio > 4, indicating that the chosen method is efficient and appropriate (Asfaram et al., 2016)For our data, we found that the CCD's signal/noise ratio is an excellent 25.1, confirming that the model can be applied to the complete previously defined design space.

The results visualized with contour plots (Figure 6) give a clear and intuitive

understanding of the correlations between adsorption and the various parameters (Montgomery, 2013). Both cyanide concentration and pH impact adsorption, i.e., greater cyanide loading and higher pH reduce adsorption. Contact time and nanoparticle adsorbent have a positive effect on adsorption, which is logical as the number of adsorption sites and a longer time for adsorption are beneficial, which is also the reason for the negative correlation between cyanide concentration and adsorption. The negative correlation between pH and adsorption in the investigated range could be due to weaker H-bonding and π-π interactions and, consequently, less likely adsorption. The reason for the reduction of these supramolecular interactions is plentiful hydroxyl groups on the green nanocomposite surface undergoing a negative transformation at higher pHs, thus leading to a lower affinity between them and cyanide.

Based on the CCD and ANOVA analysis, under the application of a non-linear optimization approach according to Nelder-Mead, the optimum parameters were found to be pH=8, 60 mg of green-prepared nanocomposite, and 60 min contact time to obtain an above 90% removal efficiency for a 50 $mg.L^{-1}$ cyanide solution. This agrees with the experiment, which found 93.0±7.1% vs. 91.7±6.2% in the model predicted (95% confidence level), showing excellent agreement between the experiment and the model.

Table 2. ANOVA table for modeling of the cyanide removal efficiency procedure.

	Sum of Square	Degree of Freedom	Mean Square	F-Value	p-Value
Block	220.8	2	110.4	2.9	0.0706
Model	12053.0	8	1506.6	40.2	0.0001
A	2703.0	1	2703.0	72.2	0.0001
B	4296.1	1	4296.1	114.7	0.0001
C	2454.3	1	2454.3	65.5	0.0001
D	291.9	1	291.9	7.8	0.0099
AB	669.5	1	669.5	17.9	0.0003
BC	145.8	1	145.8	3.9	0.0596
A^2	1115.9	1	1115.9	29.8	0.0001
C^2	376.5	1	376.5	10.0	0.0040
Residuals	936.3	25	37.4		
Lake of Fit	738.3	16	46.1	2.1	0.1304
Pure Error	197.8	9	22.0		
Cor Total	13279.6	35			

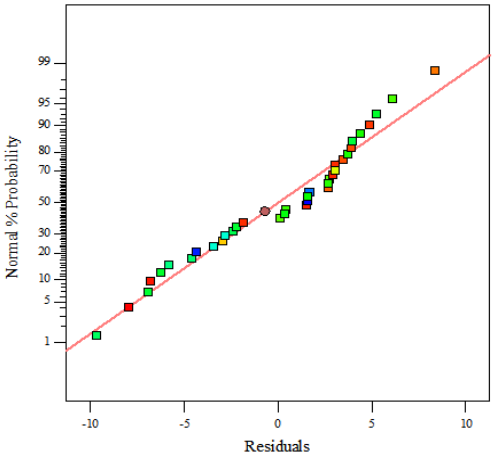

Fig 5. Normal plot of residuals for cyanide removal using the synthesized NiFe2O4-chitosan nanocomposite.

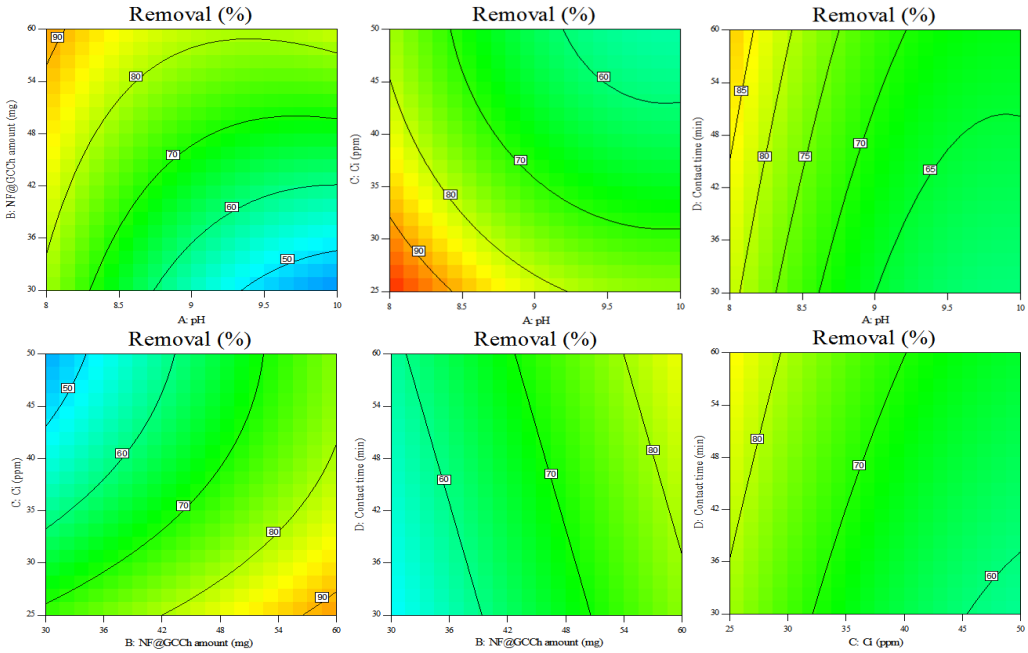

Fig 6. Contour plots, visualizing the effects of pH, nanocomposite amount, starting concentration, and contact time effects on efficiency of the adsorbent.

Adsorption isotherms

Further experiments were all done using the optimized conditions determined above. In addition to providing insight into how adsorbate interacts with adsorbent surfaces, adsorption isotherms can also contribute to determining adsorption efficiency and capacity. A variety of models have been used to describe adsorption behaviors in similar studies such as Langmuir, Freundlich, and Temkin (Gupta et al., 2012; Tanhaei et al., 2015). Analyzing the cyanide adsorption process on the synthesized nanocomposite was done using these models.

Adsorption isotherms were determined by varying the cyanide concentration (Figure 7) to gain a more in-depth insight into the physical-chemical processes behind this adsorption. For this purpose, the adsorption capacity was defined as Eq. 4.

In a linear-linear plot (Figure 7a) the data show a nonlinear behavior. Therefore, several classical adsorption models were also applied. Namely, the isotherm models according to Langmuir, Freundlich, and Temkin were used for the evaluation (Gupta et al., 2012; Tanhaei et al., 2015).

The Freundlich isotherm

The Freundlich isotherm model (see Eq. 7) assumes less material can be adsorbed when it is already covered with non-negligible amounts of adsorbed material.

$$\ln q_e = \ln k_f + \frac{1}{n} \ln C_e \qquad (7)$$

In this model, the key parameters of kf (adsorption capacity) and n (adsorption intensity) are the Freundlich constants (Gupta et al., 2012; Tanhaei et al., 2015). Here, qe ($mg.g^{-1}$) and Ce ($mg.L^{-1}$) refer to the equilibrium amount of removed cyanide and its equilibrium concentration in final treated solution, respectively. According to Table 3, the Freundlich model failed to adequately describe adsorption behavior, particularly at high and low concentrations

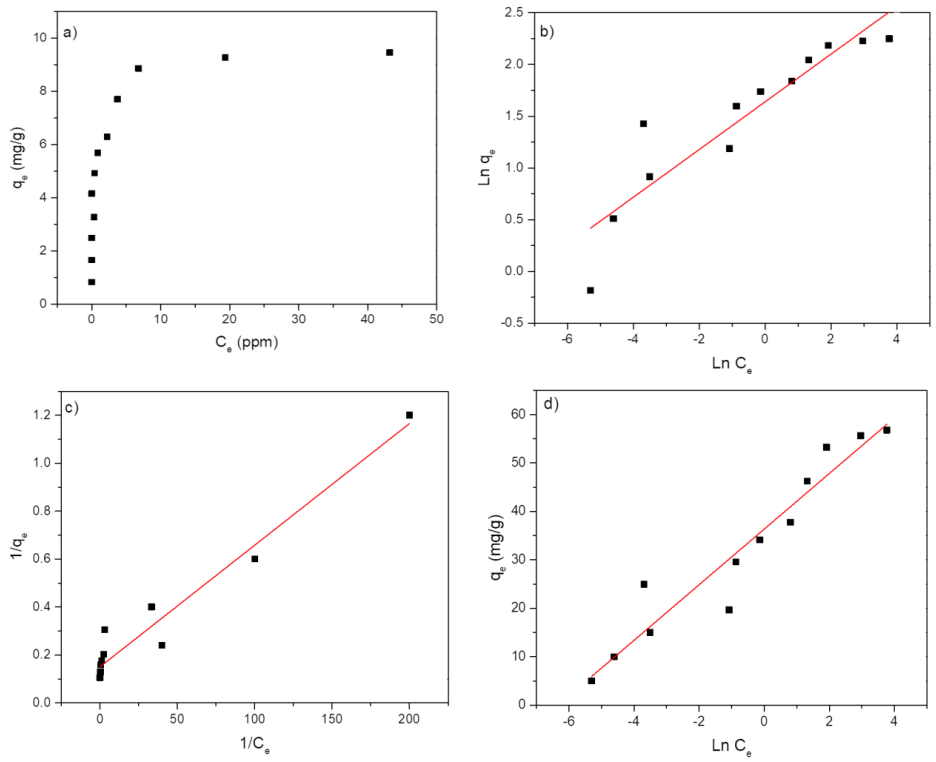

Fig 7. plots of the isotherm models; a) basic plot (qe vs. Ce), b) Freundlich model, c) Langmuir model, and d) Temkin model.

(R^2=0.8475). Even so, n = 4.3, the model parameters, indicated favorable adsorption (n > 1) (Gupta et al., 2012; Tanhaei et al., 2015).

Langmuir isotherm

The Langmuir isotherm assumes monolayer adsorption onto a surface with uniform adsorption sites and identical adsorption enthalpies for each site:

$$q_e = q_m \frac{bC_e}{1 + C_e} \quad (8)$$

where qm ($mg.g^{-1}$) is the maximum adsorption capacity, and b ($mL.mg^{-1}$) is the Langmuir constant. Typically, this equation (Eq. 8) is rearranged into linear form as follows:

$$\frac{1}{q_e} = \frac{1}{q_m} + \frac{1}{q_m b C_e} \quad (9)$$

In order to analyze adsorption favorability further, the parameter RL was calculated. For RL=0 it is irreversible, for 0 < RL< 1 it is favorable, for RL = 1 it is linear, and for RL> 1 it is unfavorable (Tanhaei et al., 2015).

$$R_L = \frac{1}{1 + bC_0} \quad (10)$$

where C0 represents the initial cyanide concentration. 60 mg of the nanocomposite was incorporated into a 10 mL solution to study cyanide adsorption at concentrations ranging from 5 to 100 $mg.L^{-1}$ (Table 3). RL value of 0.2485 and excellent fit (R^2=0.9532) indicate favorable adsorption. Langmuir's superior fit suggests monolayer adsorption with homogeneous active sites, which is the most suitable model for explaining cyanide adsorption on synthesized nanocomposite.

Table 3. Adsorption parameters of cyanide by proposed nanocomposite for Langmuir, Freundlich, and Temkin models.

T (K)	Langmuir constant				Freundlich constant			Temkin constant		
298	q_m	K_L	R_L	R^2	n	K_f	R^2	b_T	K_T	R^2
	6.6	29.57	0.2485	0.9532	4.3	5.15	0.8475	431.53	311.47	0.9242

The Temkin isotherm

According to the Temkin isotherm, the enthalpy of adsorption decreases linearly with surface coverage because adsorption sites are not identical (Anbia & Salehi, 2012; Tanhaei et al., 2017). This can be expressed as follows:

$$q_e = \frac{RT}{b_T}\ln(K_{Te}C_e) \quad (11)$$

where T (K) is temperature, R = 8.314 J/(mol·K) is the gas constant, KTe ($L\cdot g^{-1}$) is the Temkin equilibrium binding constant, and bT ($J\cdot mol^{-1}$) is the heat of adsorption (Asfaram et al., 2017; Tanhaei et al., 2017). It is often expressed as a linear equation:

$$q_e = A + B\ln C_e, \qquad A = \frac{RT}{b_T}\ln K_{Te}, \qquad \text{and } B = \frac{RT}{b_T} \quad (12)$$

With an R^2 = 0.9242, the Temkin model fit the data, but the obtained parameters indicated that the adsorption enthalpy did not decrease significantly with surface coverage. It is evident that adsorption sites remain available even at high concentrations, confirming that the Langmuir model provides the most accurate description of adsorption.

Comparison of Isotherm Models

A summary of the adsorption parameters is provided in Table 3. The Langmuir isotherm showed the best fit (R^2 = 0.9532), suggesting monolayer adsorption on a homogeneous surface. Accordingly, the nanocomposite's adsorption sites are uniform, and the maximum adsorption capacity was not reached within the studied range, confirming the material's high cyanide removal efficiency.

Kinetic studies

Identifying the mechanism and rate-controlling steps of the cyanide adsorption process requires understanding the adsorption kinetics. In order to analyze the kinetic behavior, two commonly used models were applied: pseudo-first-order and pseudo-second-order.

Pseudo-first-order model

According to the pseudo-first-order model (Wu et al., 2001), the rate of adsorption depends on the difference between equilibrium adsorption capacity (qe) and the amount of adsorbate adsorbed at time t. As the most straightforward model, a first-order model

$$\frac{dq}{dt} = k_1(q_e - q_t) \quad (13)$$

which was integrated to form (Wu et al., 2001).

$$\log(q_e - q_t) = \log q_e - \frac{k_1 t}{2.303} \quad (14)$$

Using eq. 13, the plot of log ($q_e - q^t$) versus time (Figure 8) resulted in a first-order rate constant of k_1=0.0069 min^{-1} with a

calculated q_e = 2.25 mg.g^{-1} which was determined for a 50 mg.L^{-1} initial cyanide concentration (see Table 4 and Figure 8a). This model, however, fails to adequately describe the experimental data based on the correlation coefficient R^2 = 0.7185. Figure 8a confirms this visually, indicating that the adsorption process is not pseudo-first-order.

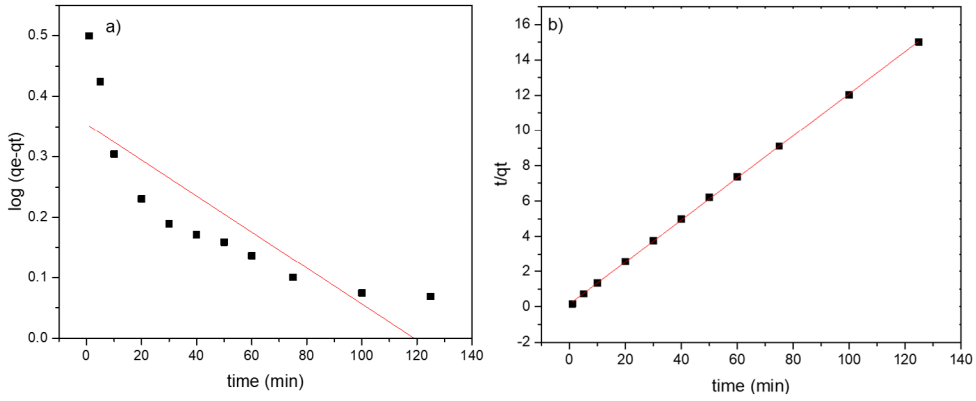

Fig 8. a) Pseudo-first-order and b) pseudo-second-order kinetic models for cyanide adsorption on proposed nanocomposite.

Table 4. Kinetics parameters for cyanide removal by proposed nanocomposite.

Time range (min)	C_0 (mg.L^{-1})	Pseudo first order			Pseudo second order		
		q_e (mg.g^{-1})	k_1 (min^{-1})	R^2	q_e (mg.g^{-1})	k_1 (min^{-1})	R^2
1-125	50	2.25	0.0069	0.7185	8.39	0.0887	0.9998

Pseudo-second-order model

In order to improve the kinetic description, a pseudo-second-order model was used. This model assumes that chemisorption, involving valency forces through electron sharing or exchange, is the rate-limiting step (Ho & McKay, 2000). The pseudo-second-order model, defined as

$$\frac{dq}{dt} = k_2(q_e - q_t)^2 \qquad (15)$$

was integrated from q = 0 to qt at t = 0 to t0 yields

$$\frac{1}{q_t} = \frac{1}{k_2 q_e^2} + \frac{t}{q_e} \qquad (16)$$

In this model, k_2 (g.mg^{-1}.min^{-1})) is the second-order rate constant. A plot of t/q_t versus t (Figure 8b) provided a straight line with R^2 = 0.9998, confirming an excellent fit to the experimental data (see Table 4 and Figure 8b).

$$h = k_2 q_e^2 \qquad (17)$$

The calculated equilibrium adsorption capacity was q_e = 8.39 mg·g^{-1}, which is very close to the experimentally observed value. This suggests that the pseudo-second-order model reliably describes the adsorption mechanism. Based on the good agreement with this model, the adsorption process is controlled by chemisorption, as in other studies on cyanide removal using nanocomposite materials (Rezaei et al., 2018; Tanhaei et al., 2015). Furthermore, it indicates that NiFe2O4 and chitosan nanocomposites have a strong affinity for cyanide ions.

Comparison of Kinetic Models

As shown in Table 4, the pseudo-second-order model offers a better fit than the pseudo-first-order model based on the kinetic parameters. This suggests that adsorption involves surface interactions and chemical bonding, rather than simple physical adsorption. The initial fast uptake followed by slower adsorption over time is consistent with other reports on chemisorptive processes (Gupta et al., 2012; Ho & McKay, 2000).

Comparison of Adsorbents for Cyanide Removal

According to Table 5, the GNF@GCCs synthesized in this study demonstrated an adsorption capacity of 8.4 $mg.g^{-1}$ at pH 8–9, which is comparable to conventional adsorbents such as activated carbon (7.0 mg.g-1, (Monser & Adhoum, 2002)) or granular activated carbon (7.9 mg/g^{-1}, (Dash et al., 2009b)). It may be environmentally and economically unfavorable to use heavy metals in certain metal-impregnated carbons, such as Cu-impregnated or Ag-impregnated activated carbon (Baghel et al., 2006; Barakat, 2005; Deveci et al., 2006; Monser & Adhoum, 2002).

GNF@GCCs nanocomposite offers a sustainable alternative through eco-friendly synthesis, magnetic separability, and biocompatibility. As a result of its moderate adsorption capacity, ease of separation, and environmental safety, it is an ideal cyanide remover for real-world applications.

Conclusion

A novel hybrid nanocomposite of green synthesized nickel ferrite (NF) coated with cross-linked chitosan as a cost-effective and eco-friendly adsorbent has been developed to remove cyanide from aqueous media. The bath adsorption experimental results demonstrated that the proposed GNF@GCCs nanocomposite exhibited exceptionally high cyanide removal efficiency at intermediate pH, making it suitable for practical water and wastewater treatments. The process reached adsorption equilibrium, with removal efficiencies above 95%, within 60 minutes, indicating its potential for real-time water and wastewater treatment. The central composite design (CCD) and ANOVA provided a robust statistical framework for optimizing the process parameters, achieving maximum cyanide removal efficiency, and a high correlation coefficient (R^2 = 0.9462). Moreover, response surface 3D plots were used to

Table 5. Comparison of the proposed GNF@GCCs with other adsorbents

Adsorbent	Adsorption capacity ($mg.g^{-1}$)	Sample pH	Reference
Activated carbon	7.0	11	(Monser & Adhoum, 2002)
Granular activated carbon	7.9	9	(Dash et al., 2009b)
TiO_2	13.0	7	(Barakat, 2005)
Ni-impregnated activated carbon	15.4	11	(Monser & Adhoum, 2002)
Cu(II)-impregnated activated carbon	16.6	10.5	(Baghel et al., 2006)
Cu-impregnated activated carbon	19.7	10.5-11	(Deveci et al., 2006)
Ag-impregnated activated carbon	26.5	11	(Monser & Adhoum, 2002)
GNF@GCCs	8.4	8-9	This study

illustrate the influence of key parameters on removal efficiency, aiding in the adsorption process optimization. The process reached adsorption equilibrium after 60 minutes for a sample containing 10 mL of 50 mg.L^{-1} cyanide at pH 8 with only 60 mg of GNF@GCCs, making it sufficiently rapid for practical application. The Langmuir isotherm model best fitted the data, confirming monolayer cyanide adsorption on a homogeneous GNF@GCCs surface. The kinetic data showed a well-fitting with a pseudo-second-order kinetic model, suggesting an initial rapid adsorption phase followed by gradual internal diffusion. Overall, this study demonstrates the effectiveness of the NF-chitosan nanocomposite as a sustainable and highly efficient adsorbent for cyanide removal, providing a viable alternative to conventional treatment methods while minimizing secondary pollution and operational costs.

References

Anbia, M. & Salehi, S. (2012). Removal of acid dyes from aqueous media by adsorption onto amino-functionalized nanoporous silica SBA-3. *Dyes and Pigments*, 94(1), 1–9. https://doi.org/10.1016/j.dyepig.2011.10.016

Asfaram, A., Ghaedi, M., Azqhandi, M. H. A., Goudarzi, A. & Dastkhoon, M. (2016). Statistical experimental design, least squares-support vector machine (LS-SVM) and artificial neural network (ANN) methods for modeling the facilitated adsorption of methylene blue dye. *RSC Advances*, 6(46), 40502–40516. https://doi.org/10.1039/c6ra01874b

Asfaram, Arash, Ghaedi, M., Ahmadi Azqhandi, M. H., Goudarzi, A. & Hajati, S. (2017). Ultrasound-assisted binary adsorption of dyes onto Mn@ CuS/ZnS-NC-AC as a novel adsorbent: Application of chemometrics for optimization and modeling. *Journal of Industrial and Engineering Chemistry*, 54. https://doi.org/10.1016/j.jiec.2017.06.018

Baghel, A., Singh, B., Pandey, P., Dhaked, R. K., Gupta, A. K., Ganeshan, K. & Sekhar, K. (2006). Adsorptive removal of water poisons from contaminated water by adsorbents. *Journal of Hazardous Materials*, 137(1), 396–400. https://doi.org/10.1016/j.jhazmat.2006.02.070

Barakat, M. A. (2005). Adsorption behavior of copper and cyanide ions at TiO2-solution interface. *Journal of Colloid and Interface Science*, 291(2), 345–352. https://doi.org/10.1016/j.jcis.2005.05.047

Beasley, D. M. G. & Glass, W. I. (1998). Cyanide poisoning: pathophysiology and treatment recommendations. *Occupational Medicine*, 48(7), 427–431. https://doi.org/10.1093/OCCMED/48.7.427

Bhatnagar, A. & Sillanpää, M. (2009). Applications of chitin- and chitosan-derivatives for the detoxification of water and wastewater - A short review. In *Advances in Colloid and Interface Science,* 152(1–2), 26–38. https://doi.org/10.1016/j.cis.2009.09.003

Chang, E. E., Hsing, H. J., Chiang, P. C., Chen, M. Y. & Shyng, J. Y. (2008). The chemical and biological characteristics of coke-oven wastewater by ozonation. *Journal of Hazardous Materials*, *156*(1–3), 560–567. https://doi.org/10.1016/j.jhazmat.2007.12.106

Dash, R. R., Gaur, A. & Balomajumder, C. (2009a). Cyanide in industrial wastewaters and its removal: A review on biotreatment. In *Journal of Hazardous Materials,* 163(1), 1–11. https://doi.org/10.1016/j.jhazmat.2008.06.051

Dash, R. R., Balomajumder, C. & Kumar, A. (2009b). Removal of cyanide from water and wastewater using granular activated carbon. *Chemical Engineering*

Journal, 146(3), 408–413. https://doi.org/10.1016/j.cej.2008.06.021

Deveci, H., Yazici, E. Y., Alp, I. & Uslu, T. (2006). Removal of cyanide from aqueous solutions by plain and metal-impregnated granular activated carbons. *International Journal of Mineral Processing*, *79(3), 1*98–208. https://doi.org/10.1016/j.minpro.2006.03.002

Donia, A. M., Atia, A. A. & Elwakeel, K. Z. (2008). Selective separation of mercury(II) using magnetic chitosan resin modified with Schiff's base derived from thiourea and glutaraldehyde. *Journal of Hazardous Materials*, 151(2–3), 372–379. https://doi.org/10.1016/j.jhazmat.2007.05.083

Douglas C. Montgomery. (2019). Design and Analysis of Experiments, 10th Edition | Wiley. In *Wiley*.

Eletta, O. A. A., Ajayi, O. A., Ogunleye, O. O. & Akpan, I. C. (2016). Adsorption of cyanide from aqueous solution using calcinated eggshells: Equilibrium and optimisation studies. *Journal of Environmental Chemical Engineering*, *4*(1), 1367–1375. https://doi.org/10.1016/j.jece.2016.01.020

Gracia, R. & Shepherd, G. (2004). Cyanide Poisoning and Its Treatment. *Pharmacotherapy: The Journal of Human Pharmacology and Drug Therapy*, 24(10), 1358–1365. https://doi.org/10.1592/PHCO.24.14.1358.43149

Gupta, V. K., Ganjali, M. R., Nayak, A., Bhushan, B. & Agarwal, S. (2012). Enhanced heavy metals removal and recovery by mesoporous adsorbent prepared from waste rubber tire. *Chemical Engineering Journal*, 197, 330–342. https://doi.org/10.1016/j.cej.2012.04.104

Hassani, G., Nasseri, S. & Gharibi, H. (2011). Removal of cyanide by electrocoagulation process. *Analytical and Bioanalytical Electrochemistry*, *3*(6), 625–634.

Hendry-Hofer, T. B., Ng, P. C., Witeof, A. E., Mahon, S. B., Brenner, M., Boss, G. R. & Bebarta, V. S. (2019). A Review on Ingested Cyanide: Risks, Clinical Presentation, Diagnostics, and Treatment Challenges. *Journal of Medical Toxicology*, 15(2), 128–133. https://doi.org/10.1007/S13181-018-0688-Y/METRICS

Ho, Y. S. & McKay, G. (2000). The kinetics of sorption of divalent metal ions onto sphagnum moss peat. *Water Research*, 34(3), 735–742. https://doi.org/10.1016/S0043-1354(99)00232-8

Hritcu, D., Humelnicu, D., Dodi, G. & Popa, M. I. (2012). Magnetic chitosan composite particles: Evaluation of thorium and uranyl ion adsorption from aqueous solutions. *Carbohydrate Polymers*, *87*(2), 1185–1191. https://doi.org/10.1016/j.carbpol.2011.08.095

Jacob, B. P., Kumar, A., Pant, R. P., Singh, S. & Mohammed, E. M. (2011). Influence of preparation method on structural and magnetic properties of nickel ferrite nanoparticles. *Bulletin of Materials Science*, 34(7), 1345–1350. https://doi.org/10.1007/s12034-011-0326-7

Kalita, C., Boruah, P. K., Das, M. R. & Saikia, P. (2022). Facile green synthesis of nickel-ferrite-rGO (NiFe2O4/rGO) nanocomposites for efficient water purification under direct sunlight. *Inorganic Chemistry Communications*, 146, 110073. https://doi.org/10.1016/J.INOCHE.2022.110073

Kumar, A., Naushad, M., Rana, A., Inamuddin, Preeti, Sharma, G., Ghfar, A. A., Stadler, F. J. & Khan, M. R. (2017). ZnSe-WO3 nano-hetero-assembly stacked on Gum ghatti for photo-degradative removal of Bisphenol A: Symbiose of adsorption and photocatalysis. *International Journal of Biological Macromolecules*, *104*, 1172–1184. https://doi.org/10.1016/j.ijbiomac.2017.06.116

Kuyucak, N. & Akcil, A. (2013). Cyanide and removal options from effluents in gold mining and metallurgical processes. In *Minerals Engineering,* 50-51,13-29. https://doi.org/10.1016/j.mineng.2013.05.027

Luque-Almagro, V. M., Moreno-Vivián, C. & Roldán, M. D. (2016). Biodegradation of cyanide wastes from mining and jewellery industries. In *Current Opinion in Biotechnology,* 38, 9–13. https://doi.org/10.1016/j.copbio.2015.12.004

Moghaddam, A. Z., Jazi, M. E., Allahrasani, A., Khazaei, M., Ganjali, M. R., Saeb, M. R. & Vatanpour, V. (2020). Removal of Chromate and Nitrate Ions from Aqueous Solutions by CoxFe3-xO4@ silica Hybrid Nanoparticles Decorated with Cross-Linked Tragacanth Gum: Experiment, Modeling and Optimization. *ChemistrySelect*, *5*(18), 5404–5413. https://doi.org/10.1002/SLCT.202000725

Monser, L. & Adhoum, N. (2002). Modified activated carbon for the removal of copper, zinc, chromium and cyanide from wastewater. *Separation and Purification Technology*, *26*(2–3), 137–146. https://doi.org/10.1016/S1383-5866(01)00155-1

Montgomery, D. C. (2013). Design and Analysis of Experiments (International Student Version). In *John Wiley & Sons, Inc*. https://doi.org/10.1198/tech.2006.s372

Moussavi, G. & Khosravi, R. (2010). Removal of cyanide from wastewater by adsorption onto pistachio hull wastes: Parametric experiments, kinetics and equilibrium analysis. *Journal of Hazardous Materials*, *183*(1–3), 724–730. https://doi.org/10.1016/j.jhazmat.2010.07.086

Munir, S., Farooq Warsi, M., Zulfiqar, S., Ayman, I., Haider, S., Alsafari, I. A., Agboola, P. O. & Shakir, I. (2021). Nickel ferrite/zinc oxide nanocomposite: Investigating the photocatalytic and antibacterial properties. *Journal of Saudi Chemical Society*, *25*(12), 101388. https://doi.org/10.1016/J.JSCS.2021.101388

Pisanic, T. R., Blackwell, J. D., Shubayev, V. I., Fiñones, R. R. & Jin, S. (2007). Nanotoxicity of iron oxide nanoparticle internalization in growing neurons. *Biomaterials*, *28*(16), 2572–2581. https://doi.org/10.1016/j.biomaterials.2007.01.043

Pulkka, S., Martikainen, M., Bhatnagar, A. & Sillanpää, M. (2014). Electrochemical methods for the removal of anionic contaminants from water - A review. In *Separation and Purification Technology.* 132,252-271. https://doi.org/10.1016/j.seppur.2014.05.021

Ramírez-Muñiz, K., Song, S., Berber-Mendoza, S. & Tong, S. (2010). Adsorption of the complex ion Au(CN)2- onto sulfur-impregnated activated carbon in aqueous solutions. *Journal of Colloid and Interface Science*, *349*(2), 602–606. https://doi.org/10.1016/j.jcis.2010.05.056

Reddy, D. H. K. & Lee, S. M. (2013). Application of magnetic chitosan composites for the removal of toxic metal and dyes from aqueous solutions. *Advances in Colloid and Interface Science*, *201–202*, 68–93. https://doi.org/10.1016/j.cis.2013.10.002

Reece, J. E., Deming, S. N. & Morgan, S. L. (1993). Experimental Design: A Chemometric Approach. In *Elsevier*.

Rezaei, R., Massinaei, M. & Zeraatkar Moghaddam, A. (2018). Removal of the residual xanthate from flotation plant tailings using modified bentonite. *Minerals Engineering*, *119*, 1–10. https://doi.org/10.1016/j.mineng.2018.01.012

Sadeghi, S., Moghaddam, A. Z. & Massinaei, M. (2015). Novel tunable composites based on bentonite and modified tragacanth gum for removal of acid dyes from aqueous solutions. *RSC Advances*, *5*(69), 55731–55745. https://doi.org/10.1039/c5ra07979a

Scarazzato, T., Buzzi, D. C., Bernardes, A. M. & Romano Espinosa, D. C. (2015). Treatment of wastewaters from cyanide-free plating process by electrodialysis. *Journal of Cleaner Production*, *91*, 241–250. https://doi.org/10.1016/j.jclepro.2014.12.046

Shadman, S., Massinaei, M. & Zeraatkar Moghaddam, A. (2021). Removal of cyanide from the gold cyanidation plant tailings using graphene-based magnetic nanocomposites. *Chemical Papers*, *75*(10), 5543–5560. https://doi.org/10.1007/s11696-021-01678-9

Sharma, G., Kumar, A., Devi, K., Sharma, S., Naushad, M., Ghfar, A. A., Ahamad, T. & Stadler, F. J. (2018a). Guar gum-crosslinked-Soya lecithin nanohydrogel sheets as effective adsorbent for the removal of thiophanate methyl fungicide. *International Journal of Biological Macromolecules*, 114, 295–305. https://doi.org/10.1016/j.ijbiomac.2018.03.093

Sharma, G., Kumar, A., Naushad, M., García-Peñas, A., Al-Muhtaseb, A. H., Ghfar, A. A., Sharma, V., Ahamad, T. & Stadler, F. J. (2018b). Fabrication and characterization of Gum arabic-cl-poly(acrylamide) nanohydrogel for effective adsorption of crystal violet dye. *Carbohydrate Polymers*, 202, 444–453. https://doi.org/10.1016/j.carbpol.2018.09.004

Singh, N. & Balomajumder, C. (2016). Simultaneous removal of phenol and cyanide from aqueous solution by adsorption onto surface modified activated carbon prepared from coconut shell. *Journal of Water Process Engineering*, *9*, 233–245. https://doi.org/10.1016/j.jwpe.2016.01.008

Tanhaei, B., Ayati, A., Lahtinen, M. & Sillanpää, M. (2015). Preparation and characterization of a novel chitosan/Al2O3/magnetite nanoparticles composite adsorbent for kinetic, thermodynamic and isotherm studies of Methyl Orange adsorption. *Chemical Engineering Journal*, 259, 1–10. https://doi.org/10.1016/j.cej.2014.07.109

Tanhaei, B., Ayati, A., Bamoharram, F. F. & Sillanpää, M. (2017). Magnetic EDTA Functionalized Preyssler Cross Linked Chitosan Nanocomposite for Adsorptive Removal of Pb(II) Ions. *Clean - Soil, Air, Water*, 45(10), 1700328. https://doi.org/10.1002/clen.201700328

Wang, J., Zheng, S., Shao, Y., Liu, J., Xu, Z. & Zhu, D. (2010). Amino-functionalized Fe3O4@SiO2 core-shell magnetic nanomaterial as a novel adsorbent for aqueous heavy metals removal. *Journal of Colloid and Interface Science*, *349*(1), 293–299. https://doi.org/10.1016/j.jcis.2010.05.010

Wu, F. C., Tseng, R. L. & Juang, R. S. (2001). Kinetic modeling of liquid-phase adsorption of reactive dyes and metal ions on chitosan. *Water Research*, *35*(3), 613–618. https://doi.org/10.1016/S0043-1354(00)00307-9

Yazici, E. Y., Deveci, H. & Alp, I. (2009). Treatment of cyanide effluents by oxidation and adsorption in batch and column studies. *Journal of Hazardous Materials*, 166(2–3), 1362–1366. https://doi.org/10.1016/j.jhazmat.2008.12.050

Zeraatkar Moghaddam, A., Ghiamati, E., Pourashuri, A. & Allahresani, A. (2018). Modified nickel ferrite nanocomposite/functionalized chitosan as a novel adsorbent for the removal of acidic dyes. *International Journal of Biological Macromolecules*, *120*, 1714–1725. https://doi.org/10.1016/j.ijbiomac.2018.09.198

Zhang, W., Liu, W., Lv, Y., Li, B. & Ying, W. (2010). Enhanced carbon adsorption treatment for removing cyanide from coking plant effluent. *Journal of Hazardous Materials*, 184(1–3), 135–140. https://doi.org/10.1016/j.jhazmat.2010.08.015